https://doi.org/10.5194/egusphere-2026-6739
Preprint. Discussion started: 13 November 2026
© Author(s) 2026. CC BY 4.0 License.

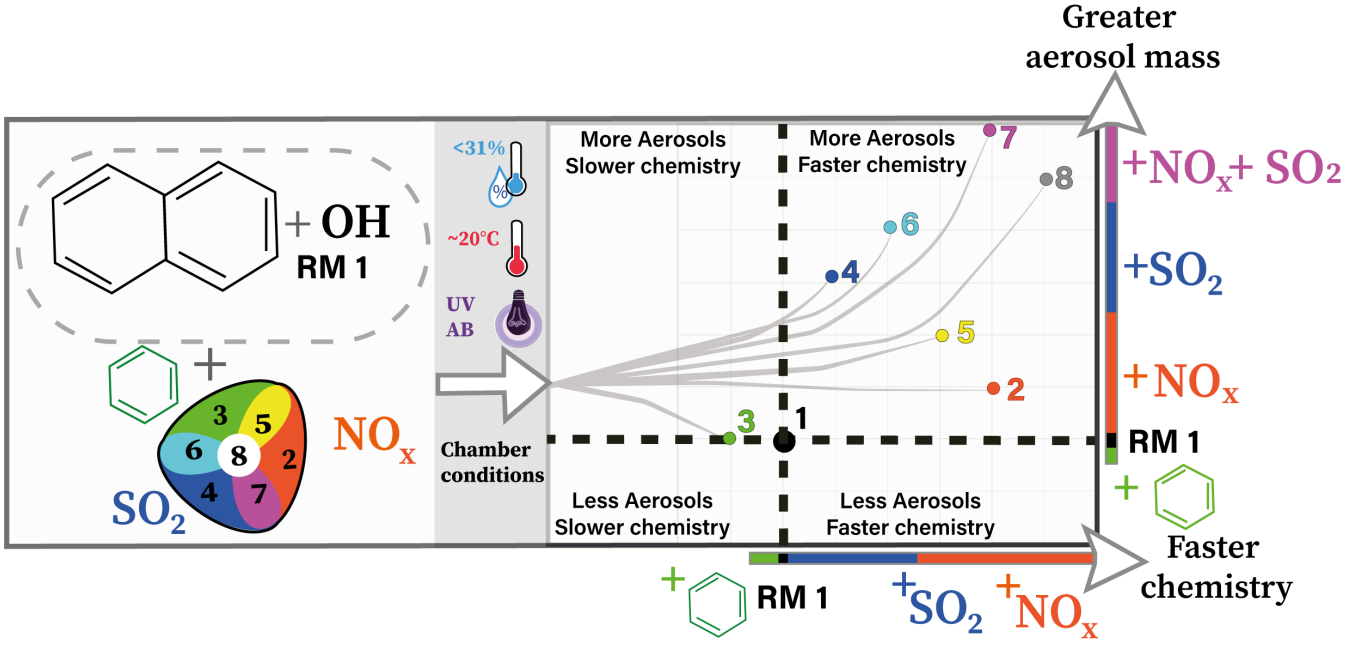
Influence of NO_x, SO_2 and benzene on the formation of secondary organic aerosol from naphthalene

Merve Polat[1,2,*], Amir Ben Brik[3,*], Niall O'Sullivan[3], Mixtli Campos-Pineda[5], Albert A. Ruth[5], John Wenger[3], Jakob K. Nøjgaard[1,2,6], and Matthew S. Johnson[2,4]

[1]National Research Centre for the Working Environment, DK-2100 Copenhagen, Denmark
[2]Department of Chemistry, University of Copenhagen, DK-2100 Copenhagen, Denmark
[3]School of Chemistry and Sustainability Institute, University College Cork, T12 YN60 Cork, Ireland
[4]Luper Technologies, NL-5656 AE Eindhoven, Netherlands
[5]School of Physics and Sustainability Institute, University College Cork, T12 YN60 Cork, Ireland
[6]Department of Environmental Science, Aarhus University, DK-4000 Roskilde, Denmark
[*]*These authors contributed equally*

Correspondence: Matthew S. Johnson (msj@chem.ku.dk)

Graphical abstract:



https://doi.org/10.5194/egusphere-2026-6739
Preprint. Discussion started: 13 November 2026
© Author(s) 2026. CC BY 4.0 License.



Abstract. Naphthalene, the most abundant atmospheric gas-phase PAH and a known Secondary Organic Aerosol (SOA) precursor, is emitted from combustion and asphalt production and paving alongside other hydrocarbons, NO_x and SO_2. We investigated the influence of reaction conditions on the formation of SOA from the OH-oxidation of naphthalene in the Irish Atmospheric simulation Chamber (IASC). Benzene, NO_x and SO_2 were added to the chamber both individually and in combination, resulting in a total of eight reaction mixtures (RM). SOA formation was observed in all RM, with the base case of 30 ppbv of naphthalene producing 40 μg m^{-3} after 1 hour of photooxidation. The different co-reactants significantly influenced the formation and evolution of SOA: the addition of benzene delayed the onset of particle formation, whereas NO_x accelerated particle formation by promoting faster generation of oxidation products and enhanced the total particle mass concentration, likely through enhanced OH radical recycling. The addition of SO_2 accelerated particle formation by increasing the condensability of organic vapours without altering the underlying chemistry. The combined presence of NO_x and SO_2 produced the strongest effect, both accelerating oxidation product formation and enhancing partitioning into the particle phase. Our results demonstrate that studies of individual precursor systems may overlook secondary pollutant formation from mixture effects that are relevant to real-world environments. Air pollutant formation depends not only on SOA precursor emissions but also on co-oxidation with other gaseous pollutants. Reducing Volatile Organic Compounds (VOC), NO_x, and SO_2 emissions may therefore improve air quality and reduce occupational exposure.

https://doi.org/10.5194/egusphere-2026-6739
Preprint. Discussion started: 13 November 2026
© Author(s) 2026. CC BY 4.0 License.

1 Introduction

Growing urbanisation places increasing demands on construction materials, such as asphalt, which is widely used for paving roads and highways. Asphalt-related emissions occur throughout the material life cycle, such as production, paving, in-use aging, maintenance, and demolition. These emissions can affect the atmospheric environment through the release of a broad range of organic compounds, particularly volatile and semi-volatile organic compounds (VOCs and SVOCs) (Li et al. (2024)).Such compounds may be hazardous in their own right and contribute to the formation of secondary organic aerosol (SOA)(Khare et al. (2020); Kriech et al. (2022); Khare and Gentner (2018)). Consequently, asphalt emissions are relevant for both occupational exposure and public health.

Asphalt mixtures consist of bitumen, coarse aggregate, and fine aggregate, where bitumen acts as the binder and is typically derived from crude oil. Bitumen is a complex mixture of organic compounds, including numerous high-molecular-weight species and polycyclic aromatic hydrocarbons (PAHs). The chemical and physical characteristics of emitted bitumen fumes can vary depending on the activity, machinery, temperature, and materials used. Even though PAHs generally constitute only a small fraction of the total bitumen content, they are of great concern for both SOA forming potential and occupational exposure. Many studies report that PAHs are predominantly present in the gas phase (Burstyn et al. (2002); Väänänen et al. (2003)), with naphthalene often being the most abundant PAH.

Recent studies have identified key components of asphalt-related emissions at construction and demolition sites, as well as in production plants (Mousavi et al. (2024); del Carmen Rubio et al. (2013)). Compounds such as naphthalene, benzene, NO, and SO_2 are frequently reported. In addition, field studies have observed elevated particle number and mass concentrations in workers' breathing zones (Hedmer et al. (2026); Freund et al. (2012); Elihn et al. (2008)), some of which may arise from SOA formed through the atmospheric oxidation of emitted organic compounds.

Naphthalene is not only present in the air at asphalt worksites, but it is typically the most abundant PAH in the atmosphere and a significant contributor to ambient SOA, as observed during a wintertime haze event in Beijing Huang et al. (2019). Another study by Cheng et al. (2026) likewise found 2-ring PAHs, like naphthalene, to be the largest contributor to SOA in wintertime. Most existing studies have investigated naphthalene oxidation as an isolated precursor system. Here, several chamber studies have examined the OH-initiated oxidation of naphthalene (Chen et al. (2016); Chan et al. (2009); Shakya and Griffin (2010)), while others have investigated the influence of NO_x chemistry on naphthalene-derived SOA formation and composition (Chen et al. (2018); Kautzman et al. (2010); Kleindienst et al. (2012); Sari Doré et al. (2025); Riva et al. (2015)). Detailed oxidation schemes for OH driven naphthalene with and without NO_x are well described in the literature (Lannuque and Sartelet (2024)). However, real-world asphalt emissions are complex mixtures rather than single-compound systems.

A small number of laboratory studies have investigated the photo-oxidation of monoaromatic compounds in the presence of SO_2 (Zhang et al. (2020); Li et al. (2022)), but to the best of our knowledge, none have focused specifically on naphthalene co-reacting with SO_2. Similarly, only a few studies have explored systems combining SO_2 with other inorganic vapors, such as NO_x or NH_3 (Yang et al. (2020, 2021)). Furthermore, only one study has investigated naphthalene photo-oxidation in the presence of other VOCs (Chen et al. (2018)) despite these combinations of reagents occurring commonly at construction sites

https://doi.org/10.5194/egusphere-2026-6739
Preprint. Discussion started: 13 November 2026
© Author(s) 2026. CC BY 4.0 License.

and urban environments. The literature on naphthalene photo-oxidation in the presence of both organic and inorganic species is scarce. Because SOA precursors are rarely emitted individually in real atmospheric environments, it is important to study their oxidation in more relevant chemical systems. Here, we investigate naphthalene oxidation in the presence of benzene and inorganic gases relevant to asphalt-related environments, particularly asphalt plants and roadsides. The experimental design allows us to examine how co-emitted organic and inorganic compounds influence SOA formation, chemical composition, and atmospheric aging. In this manuscript, we focus on experimental SOA formation under controlled chamber conditions using the Irish Atmospheric Simulation Chamber (IASC) and how NO_x, SO_2, and benzene influence SOA from photo-oxidation of naphthalene. The investigation of the underlying chemical mechanisms and their impact on SOA composition will be presented elsewhere (Ben Brik et al., 2026).

2 Method and Materials

We investigated eight reaction mixtures (RM) in which naphthalene served as the SOA precursor and assessed the effect of adding co-reactants individually and in combination: NO_x (RM2), benzene (RM3), SO_2 (RM4), and their combinations (Figure1). In total, 26 experiments were carried out under a range of different initial conditions. (Table S1). Most experiments were conducted without added water vapor corresponding to initial relative humidity in the range 1-5%. In 10 experiments, water vapor was added to give initial RH in the range 16-31%. Initial temperatures were typically 19 °C, gradually increasing to around 21 °C as the reactions progressed. RM1 (naphthalene + OH) is referred to as the base case, and RM8 includes all components (naphthalene, OH, benzene, NO_x, and SO_2).

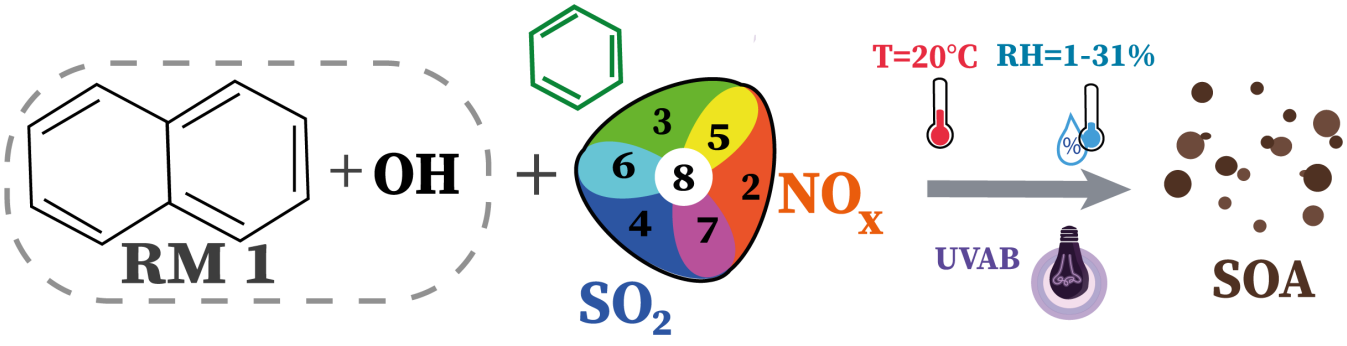


Figure 1. Overview of the reaction mixtures (RM) investigated in this study, with naphthalene as the SOA precursor. RM1 is the reference case containing only naphthalene and OH. For example, RM2 includes the addition of NO_x, RM3 includes benzene, and RM5 includes both NO_x and benzene.

https://doi.org/10.5194/egusphere-2026-6739
Preprint. Discussion started: 13 November 2026
© Author(s) 2026. CC BY 4.0 License.

2.1 Experimental setup and procedure

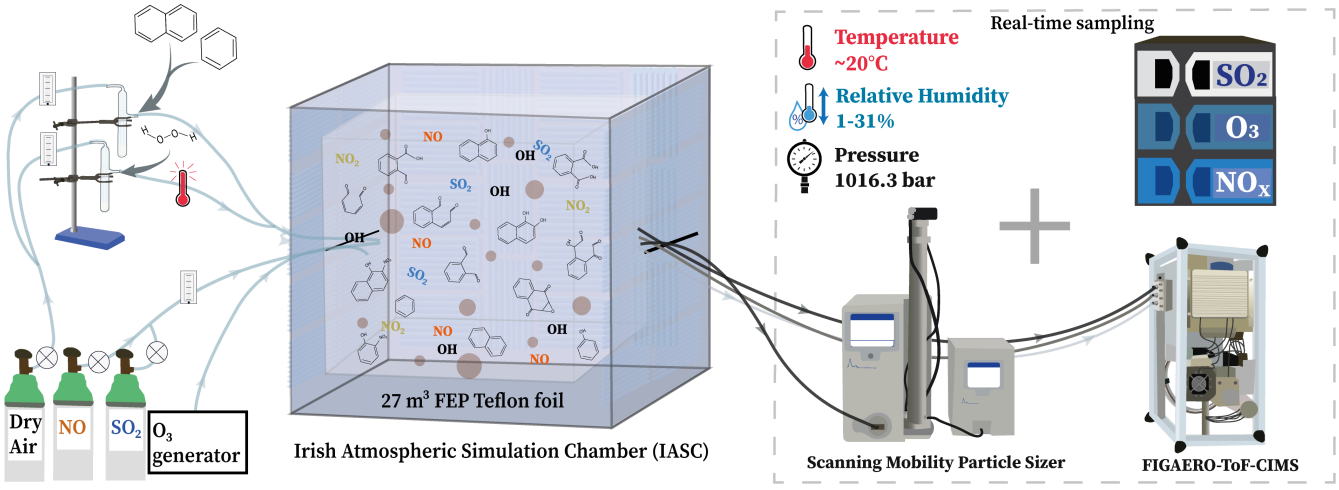


Figure 2. Schematic of the IASC. The left side shows the arrangement for addition of gases (NO_x, SO_2 and O_3) and vapors (H_2O_2, naphthalene and benzene) to the chamber. The right side shows the key instruments used for analysis in this work, including the Scanning Mobility Particle Sizer (SMPS), Time of Flight Chemical Ionization Mass Spectrometer (ToF-CIMS) and gas analyzer.

Experiments were conducted in the IASC (Figure 2), a 27 m^3 FEP Teflon-foil chamber supported by an aluminium frame and surrounded by 140 UV lamps (98 UVA lamps and 42 UVB lamps) for photolysis of OH radical precursors. The cuboidal chamber was located inside an air-conditioned enclosure, where a ventilation system controlled the ambient temperature to within 1 K of the set temperature of 293 K. The side walls were equipped with mounting plates with various port sizes, allowing introduction of reagents and sampling of the gas mixtures for analysis. An air purification system equipped with a drier, two charcoal filter towers, and two HEPA filters was connected to an air compressor to remove water vapour, VOCs, NO_x, and particles, respectively, prior to delivery to the chamber. When not in use, the chamber was continuously flushed with purified air at 1000 L min^{-1}. Before running experiments, the chamber was chemically cleaned by humidifying it and photolyzing a high mixing ratio of O_3, typically in excess of 200 ppbv. O_3 was generated using a VMUS-4 ozone generator (Oxidation Technologies). After cleaning, the chamber was switched to Experiment mode, where the pressure was maintained at 10 Pa above ambient by adding clean air to replace the air that had been extracted from the chamber by the various instruments. If required, water vapor was added to the chamber using a custom-built humidification system. The reaction-mixture components were introduced in the dark to allow complete mixing and volatilization. The following species were used to generate the eight reaction mixtures: H_2O_2 (Sigma-Aldrich, 50 wt.% in H_2O), which acts as the OH precursor (via H_2O_2 photolysis, Figure S4), naphthalene (Sigma-Aldrich Fluka, >99.0% purity), benzene (Sigma-Aldrich Fluka, >99.5% purity), and NO (Air Liquide, 99 ppmv NO in N_2); SO_2 (BOC gases, 100 ppmv SO_2 in synthetic air) and water vapour produced by the chamber humidification system. The inorganic gases, NO_x, SO_2 and O_3 were continuously monitored using automated gas analysers (Teledyne T200 for NO_x, T100 for SO_2 and T400 for O_3) operating at 1 minute time resolution.

https://doi.org/10.5194/egusphere-2026-6739
Preprint. Discussion started: 13 November 2026
© Author(s) 2026. CC BY 4.0 License.

2.2 SMPS measurements

The scanning mobility particle sizer (SMPS, TSI 3938 with a TSI 3082 electrostatic classifier and TSI 3750 condensation particle counter) provided measurements of particle size distributions and number concentrations. To interpret the particle properties measured by the SMPS, several calculations were performed. Particle mass concentrations were estimated assuming a particle density of 1.5 g cm^{-3} (Chan et al., 2009). The coagulation rate (r_{coag}) was calculated following Seinfeld and Pandis 2016 and is described in detail in supplementary Section S2.1. These calculations resulted in a size-resolved coagulation sink comparable to the measured number (dN) and mass (dM) distributions. The size-resolved r_{coag} was subsequently summed at each time step across all particle diameters to obtain the total coagulation sink, r_{coag}, which is the value reported in this work. Particle growth rates (r_{growth}) were derived to characterise the evolution of newly formed particles. The original SMPS size distribution consists of 102 mobility-diameter bins. To improve the signal-to-noise ratio, these were grouped into seven broader bins, from which growth rates were calculated. These are described in more detail in Section S2.2.

2.3 ToF-CIMS measurements

Naphthalene and its oxidation products were measured using a ToF-CIMS (Aerodyne C4Q-106) fitted with a Filter Inlet for Gases and Aerosols (FIGAERO) to allow for the analysis of species in both the gas and particle phases. The instrument was operated in both positive and negative ion modes, using toluene (C_7H_8) and methyl iodide (CH_3I) to produce $C_7H_8^+$ and I^- reagents, respectively, for the detection of a wider range of oxidation products. Negative mode (I^-) was used to detect more electronegative compounds. In positive mode ($C_7H_8^+$), the instrument was sensitive to the primary SOA precursor (naphthalene), whereas in negative mode naphthalene was not detected. Data from the ToF-CIMS were further processed by generating time-series plots for each experiment. ToF-CIMS and SMPS data were combined to examine the evolution of individual species relative to their baseline signal, defined as the signal measured five minutes before the UVA and UB (UVAB) lamps were switched on. Only species exhibiting a discernible maximum were included in the analysis. Two metrics were calculated for each peak: (1) the maximum intensity, defined as the increase in signal relative to the baseline, and (2) the time to peak, defined as the elapsed time between activation of the UVAB lamps and the occurrence of the maximum signal. The time to peak was used as a proxy for the relative rate of species formation across the different experiments, providing a basis for assessing whether product formation occurred more slowly or more rapidly among the different reaction mixtures.

2.4 Initial experiment conditions, and the estimation of OH concentrations and production rates

Data from the ToF-CIMS and gas analysers were further processed to determine the initial conditions for each experiment and to calculate OH concentrations and production rates. The supplementary Section S4 provides time-series plots for each experiment (Figures S22-S48). Because the ToF-CIMS was operated in two ionisation modes, naphthalene was not measured directly in all experiments. 8 out of 26 experiments were conducted in positive-ion mode, in which naphthalene could be detected (Table S1). Although the same mass of naphthalene ($\sim$ 5 mg) was weighed for each experiment, the exact amount transferred to the chamber varied slightly, as indicated by differences in the ToF-CIMS signal (Figure S19). The initial naphthalene levels were

https://doi.org/10.5194/egusphere-2026-6739
Preprint. Discussion started: 13 November 2026
© Author(s) 2026. CC BY 4.0 License.



therefore adjusted based on the relative ToF-CIMS response and the amount of naphthalene introduced into each experiment. For the remaining 18 experiments conducted in negative mode, naphthalene was not detected directly, and this adjustment could therefore not be applied. The ozone monitor also exhibited cross-sensitivity to several chamber constituents, including benzene, naphthalene (Spicer et al., 2010), and H_2O_2, because they absorb the 254 nm radiation emitted by the mercury lamp inside the instrument (Figure S13). Prior studies have also reported a correlation between ozone monitor readings and H_2O_2 concentration (Abue et al., 2024). A model was therefore fitted to the measured pre-illumination maximum ozone signal to estimate the individual contributions from the different interfering compounds. The model provided reasonable estimates of the initial naphthalene and benzene concentrations during the pre-illumination period. Model development and evaluation are described in greater detail in Section S3.1 and presented in Figures S13-S18. The OH concentration was determined using two complementary approaches. The 8 experiments conducted in positive mode enabled OH concentrations to be derived from the observed decay of naphthalene, assuming first order decay kinetics (see Section S3.2). When benzene was present, its additional contribution to OH loss was included as described in Eq. S10. For experiments conducted in negative mode, naphthalene was not measured directly and OH could therefore not be determined from its decay. Instead, OH concentrations were estimated using an empirical proxy model (see Section S3.3 and Figure S20). The proxy was trained using experiments for which naphthalene-decay-derived OH concentrations were available and related the OH concentration to variables relevant to OH production and loss, including the initial concentrations of benzene, H_2O_2, naphthalene, and NO_x. The OH production rate (r_{OH}) was subsequently calculated using either the OH concentration derived from the experimentally measured decay of naphthalene, or the OH concentration derived from the model. An effective pseudo-first-order OH loss rate coefficient was calculated by accounting for reactions of OH with naphthalene, benzene, SO_2, and NO_2 after illumination (see Section S3.4). All derived metrics are reported in Tables S1-S3.

3 Results and discussion

A total of 26 experiments were performed on naphthalene photoxidation in the IASC under different reaction conditions, as summarised in Table S1. SOA was observed in all experiments and attributed to naphthalene photoxidation because no detectable particle formation was observed in control experiments without the PAH precursor, i.e., from photolysis of H_2O_2 in the presence of SO_2 or benzene, with and without NO_x. Additional tests on the benzene + OH reaction at elevated benzene (320 ppbv), H_2O_2, and NO_x levels also did not produce detectable particle formation. This is consistent with a previous study which only detected negligible amounts of SOA from the photoxidation of ~4000 ppbv benzene (Borrás and Tortajada-Genaro, 2012) have also only detected small, negligible amounts of SOA from photooxidation of benzene, even at elevated levels of ~4000 ppbv. However, it is interesting to note that particles were detected during tests on the reaction mixture OH + benzene + SO_2.

Experiments were conducted with an initial relative humidity of <31% and at a temperature of approximately 19 °C (Table S1). Experiments performed at higher RH generally produced less SOA than those without added water vapor. However, as shown in Figure S21, the effect is neither large nor consistent in this set of experiments, and since the humidification system

https://doi.org/10.5194/egusphere-2026-6739
Preprint. Discussion started: 13 November 2026
© Author(s) 2026. CC BY 4.0 License.

was not functioning optimally, the effect of RH on SOA formation was not investigated further. The analysis, therefore, focuses on the role of added NO_x, SO_2, and benzene on SOA formation from naphthalene, resulting in eight reaction mixtures shown in Figure 1.

3.1 Particle formation and evolution

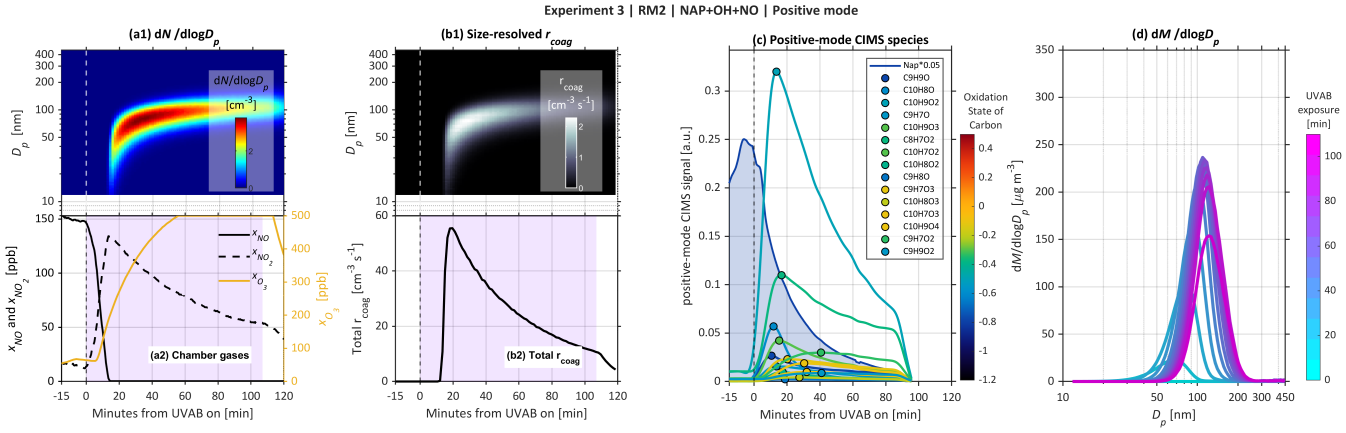


Figure 3. Example time series for RM2 (naphthalene + OH + NO_x). Panels (a) show the particle number size distribution and gas-phase concentrations, (b) the coagulation rate, and (c) selected ToF-CIMS signals (toluene reagent ion), all shown relative to UVAB lamps on ($t = 0$). Panel (d) shows the evolution of the particle mass size distribution with increasing UVAB exposure time.

Data from one of the experiments conducted on RM2 is shown in Figure 3. Reactants (here RM2: NO_x, naphthalene, and H_2O_2) are added in the dark while the chamber is in experiment mode. After the gases are mixed, the UVAB lamps are switched on, resulting in rapid new particle formation within 15 min (Figure 3.a1). As the experiment proceeds, particles coagulate (Figure 3.b) and grow to larger $dN/d\log D_p$ modes (Figure 3.d). Figure 3.c shows a selection of the gas-phase species detected by ToF-CIMS (positive mode). The naphthalene signal peaks approximately 15 minutes before the UVAB lamps are switched on and subsequently decreases gradually due to a combination of wall losses and dilution. Following illumination, the naphthalene signal decreases rapidly due to oxidation, accompanied by the formation of oxidation products. Most of these products reach their maximum signals within the first 30 minutes, as indicated by the filled circles, broadly coinciding with the observed peak times (t_{max}) for total particle number concentration (n_{PNC}) and total coagulation rate (r_{coag}). Figure 3 shows a single experiment, but equivalent data treatment was performed for all 25 other experiments (Figures S22-S47) and averaged into the eight reaction mixtures, with the results summarised in Table 1. Figures 4 and 5 show the average particle mass concentration attributed to SOA and the coagulation rate for each reaction mixture. The reaction of naphthalene with OH (RM1) yields an average SOA mass concentration of 38.3 ± 4.9 μg m^{-3}. Adding benzene (RM3) reduces the mass concentration slightly to 37.8 ± 7.3 μg m^{-3}, though not significantly, whereas adding NO_x increases it to 53.6 ± 3.8 μg m^{-3} (Table 1). Table 1 also reports the SOA mass to initial naphthalene ratio $m_{\mathrm{SOA}}/m_{\mathrm{Nap,int}}$. Here, NO_x

https://doi.org/10.5194/egusphere-2026-6739
Preprint. Discussion started: 13 November 2026
© Author(s) 2026. CC BY 4.0 License.

increases the ratio, while benzene shows no strong effect on the ratio. Figure S48 compares SOA mass concentrations from this study with two previous studies. The results obtained by Chan et al. 2009 are in agreement with this work when differences in initial naphthalene concentrations are taken into account, whereas Shakya and Griffin 2010 reported a slightly smaller increase in SOA as a function of initial naphthalene levels.

Table 1. SOA formation parameters for naphthalene oxidation obtained by averaging results (presented as Mean (SE) from several experiments under the specified conditions: SOA mass concentration (m_{SOA}), total coagulation rate (r_{coag}), particle number concentration (n_{PNC}), and the corresponding times in which they peak as t_{max}. The production of OH radicals and the $m_{SOA}/m_{Nap,int}$, where $m_{Nap,int}$ is the mass of naphthalene at the start of the reaction, is likewise shown.

RM	m_{SOA} μg / m^3	t_{max} (m_{SOA}) min	$m_{SOA}/m_{Nap,int}$	r_{OH} ($\times 10^8$) cm^{-3} s^{-1}	r_{coag} cm^{-3} s^{-1}	t_{max} (r_{coag}) min	n_{PNC} ($\times 10^5$)	t_{max} (n_{PNC}) min
1	38.3 (4.9)	105.9 (2.4)	0.24 (0.03)	3.5 (1.0)	21.2 (2.2)	20.9 (2.4)	0.8 (0.1)	20.6 (2.5)
2	53.6 (3.8)	73.3 (6.2))	0.34 (0.02)	5.5 (1.5)	43.1 (18.9)	19.1 (3.6)	1.1 (0.3)	17.8 (2.7)
3	37.8 (7.3)	109.9 (3.8)	0.24 (0.05)	3.7 (0.6)	15.0 (5.3)	24.4 (3.9)	0.7 (0.1)	22.9 (3.0)
4	50.0 (29.4)	105.5 (4.9)	0.31 (0.19)	3.4 (0.9)	160.4 (76.4)	13.3 (0.4)	2.4 (0.8)	11.8 (0.4)
5	53.8 (5.9)	88.3 (6.3)	0.34 (0.04)	6.1 (0.6)	38.4 (7.6)	17.3 (0.3)	1.1 (0.1)	16.8 (1.0)
6	76.0 (12.5)	114.0 (1.9)	0.48 (0.08)	4.1 (0.6)	348.6 (141.27)	11.3 (0.9)	4.0 (1.6)	10.5 (1.9)
7	111.2 (10.7)	64.1 (10.0)	0.70 (0.07)	4.4 (0.1)	1080.4 (911.7)	7.8 (2.6)	6.5 (3.6)	6.3 (2.6)
8	101.2 (10.8)	86.8 (20.8)	0.64 (0.07)	6.7 (0.3)	696.3 (636.5)	8.8 (3.8)	4.9 (2.9)	8.8 (3.8)

https://doi.org/10.5194/egusphere-2026-6739
Preprint. Discussion started: 13 November 2026
© Author(s) 2026. CC BY 4.0 License.

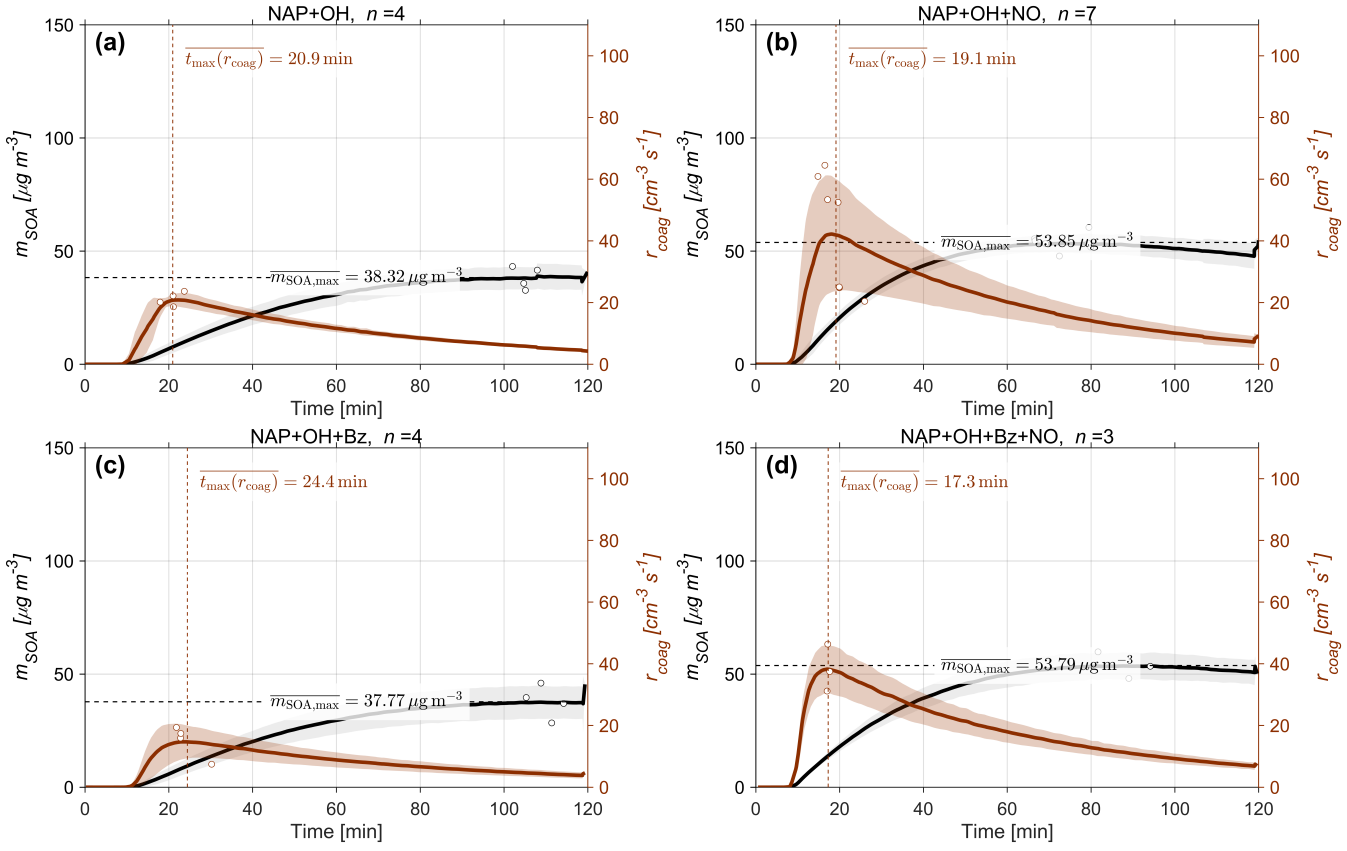


Figure 4. Average time series of particle formation from experiments on RM1, RM2, RM3 and RM5. The panels show the particle mass concentration of SOA (m_{SOA}) and the coagulation rate (r_{coag}) as a function of time, where $t = 0$ corresponds to turning UVAB lamps on. n is the number of replicate experiments performed in each RM.

https://doi.org/10.5194/egusphere-2026-6739
Preprint. Discussion started: 13 November 2026
© Author(s) 2026. CC BY 4.0 License.

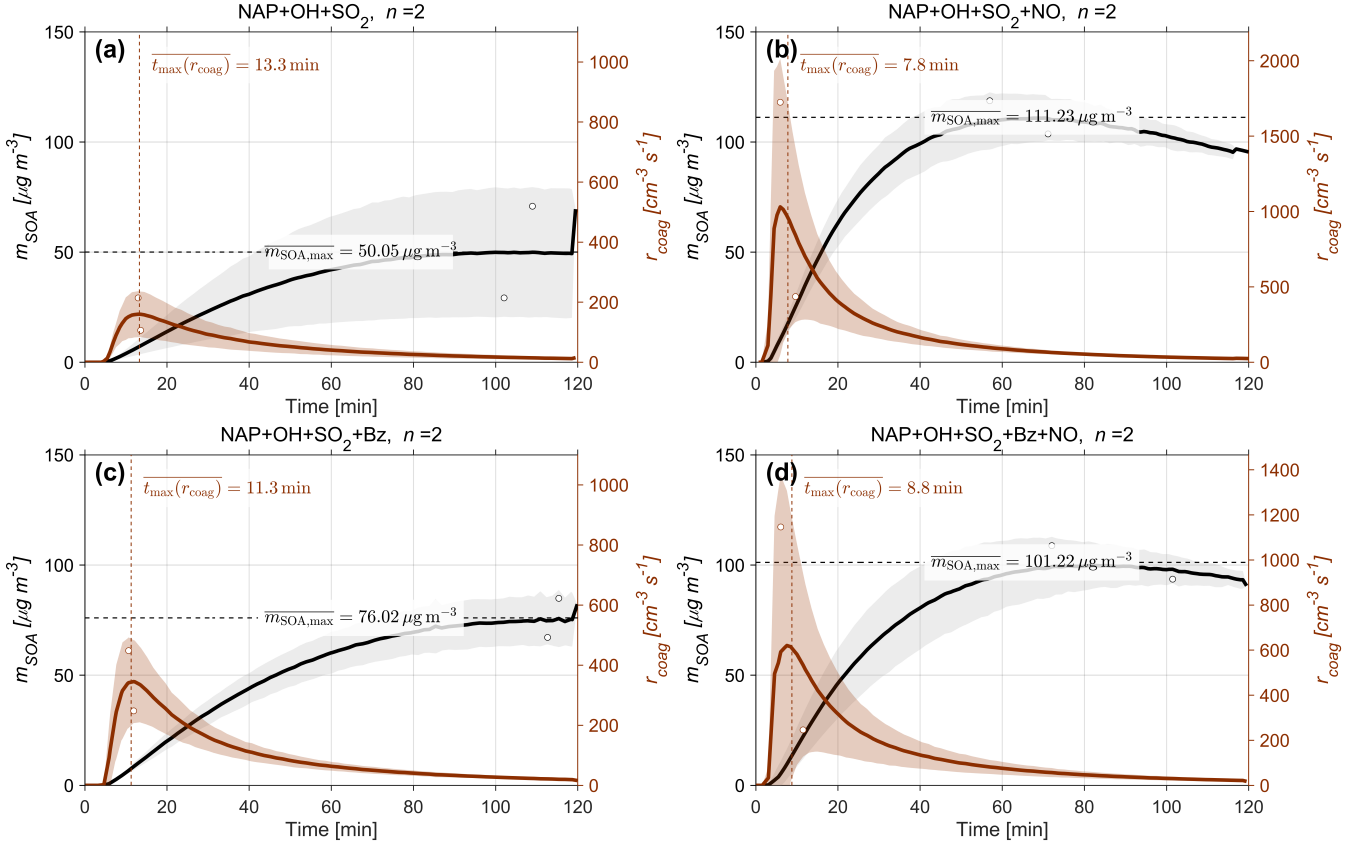


Figure 5. Average time series of particle formation from experiments on RM4 and RM6-RM8. The panels show m_{SOA} and r_{coag} as a function of time, where $t = 0$ corresponds the time when the UVAB lights are turned on. Measurement in all panels are based on two replicates.

Comparing RM2 to RM1 (Figure 4b and 4a, no $\mathrm{NO_x}$) shows that adding $\mathrm{NO_x}$ both enhances and accelerates aerosol formation. Consistent with this, gas-phase oxidation products form more rapidly in the $\mathrm{NO_x}$-containing mixtures (Figure 6), particularly when comparing RM1 and RM3 with their $\mathrm{NO_x}$-containing counterparts (RM2 and RM5). Overall, $\mathrm{NO_x}$ shifts peak times earlier for particle number concentration, r_{coag}, and most gas-phase oxidation products.

https://doi.org/10.5194/egusphere-2026-6739
Preprint. Discussion started: 13 November 2026
© Author(s) 2026. CC BY 4.0 License.

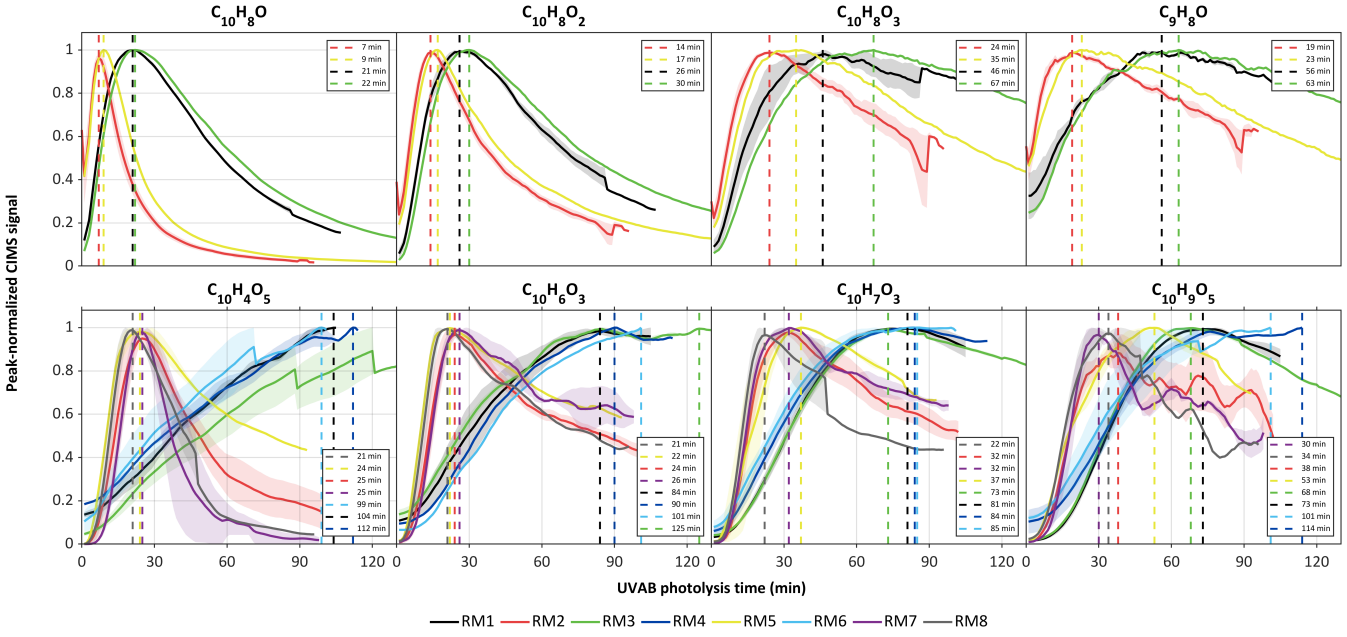


Figure 6. Formation of gas-phase oxidation products observed in positive mode (upper panel) and negative (lower panel) mode as a function of time, where $t = 0$ corresponds to the beginning of the photolysis (UVAB lamps on). Peak times are stated in the viewgraphs. Positive mode includes RM1, RM2, RM3 and RM5, whereas negative mode includes all reaction mixtures.

The ratio $m_{\mathrm{SOA}}/m_{\mathrm{Nap,int}}$ is slightly higher with $\mathrm{NO_x}$ addition (see Table 1). However, while $\mathrm{NO_x}$ substantially increases OH production (thereby accelerating particle formation), this does not translate proportionally into higher SOA mass. Benzene addition slows the formation of naphthalene oxidation products (see Figure 6). In contrast, $\mathrm{NO_x}$ significantly accelerates oxidation chemistry, with many peak times approximately halved. Adding benzene together with NO does not substantially
185 weaken the $\mathrm{NO_x}$-driven acceleration. The addition of $\mathrm{SO_2}$ strongly affects r_{coag} (see Figure 5 in comparison to Figure 4), promoting much faster particle formation but does not have a $\mathrm{SO_2}$ does not have a distinguishable effect on gas phase product peak times (Figure 6). Combining $\mathrm{SO_2}$ with benzene increases particle mass (Figure 4). Finally, when both $\mathrm{SO_2}$ and $\mathrm{NO_x}$ are present, oxidation products reach their maxima earlier than in the corresponding $\mathrm{NO_x}$-only cases.

https://doi.org/10.5194/egusphere-2026-6739
Preprint. Discussion started: 13 November 2026
© Author(s) 2026. CC BY 4.0 License.



Growth rates and particle $dN/d\log D_p$ modes

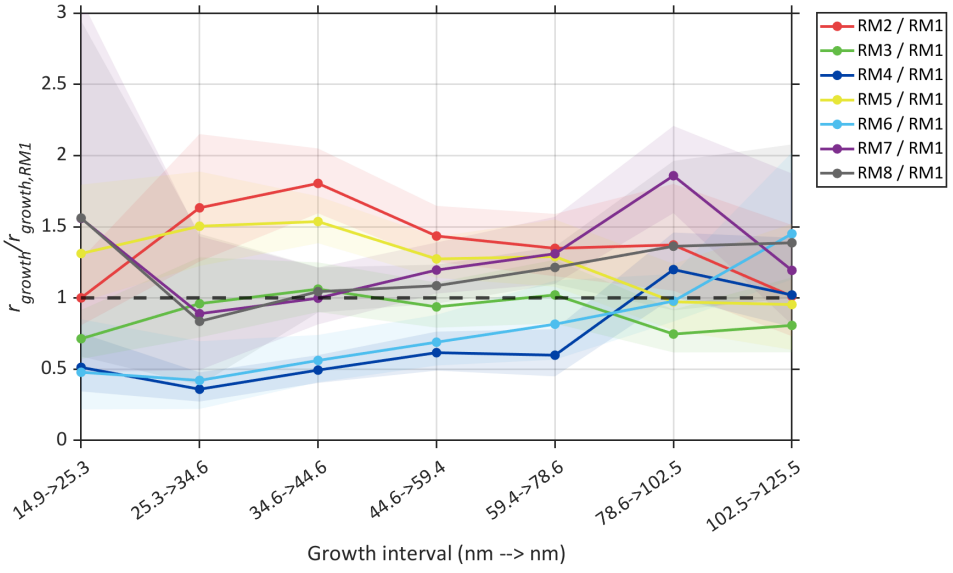


Figure 7. The ratio of growth rates between RM_i (i=2-8) and the base case. Growth-rate calculations are provided in Section S2.2.

The average SOA growth rate for each RM is shown in Figure S10, while Figure 7 presents the ratio of growth rates found for RM_i (i=2...8) and RM1. NO_x (RM2 and RM5) enhances particle growth rates, whereas the presence of SO_2 reduces growth. Thus, SO_2 accelerates particle formation (Table 1), but the resulting particle mode grows more slowly than in the other mixtures. Comparing these r_{growth} trends with the particle number size distributions in Figure 8 reveals a clear pattern. Experiments containing SO_2 (RM4 and RM6-RM8) exhibit intense particle formation within the first 0-10 min. Particle number concentrations in these cases are approximately 200-250 times higher than in RM1. During this early stage, the particle mode diameter is similar to, or slightly larger than, that of RM1.

https://doi.org/10.5194/egusphere-2026-6739
Preprint. Discussion started: 13 November 2026
© Author(s) 2026. CC BY 4.0 License.

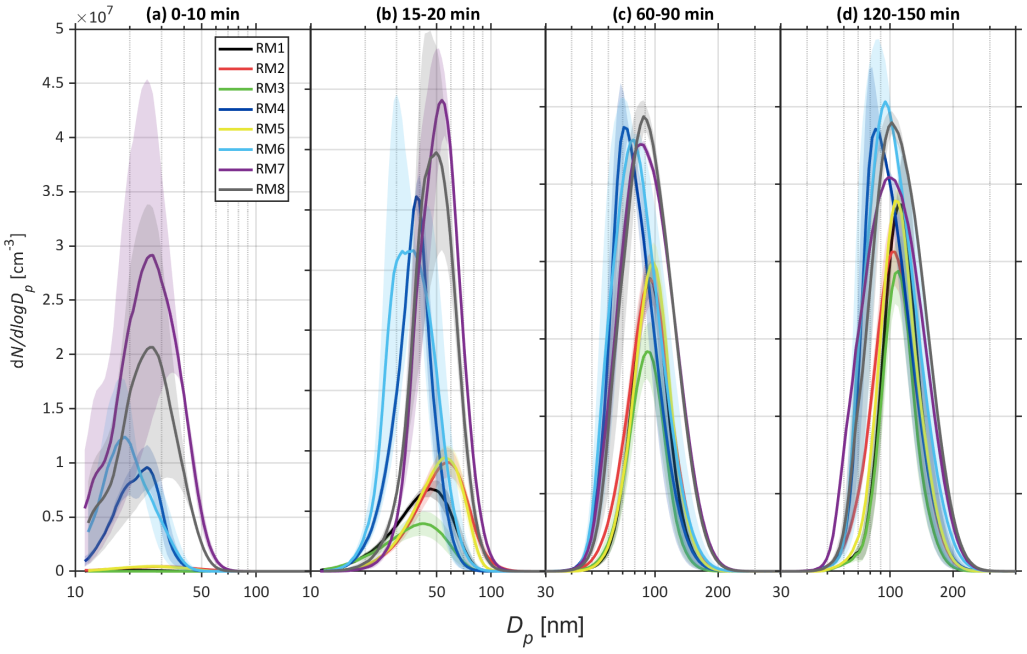


Figure 8. Particle number size distributions ($dN/d\log D_p$) averaged over replicates for each reaction mixture and shown for four time windows after UVAB lights-on. The x-axis limit for panels a and b is 10-200 nm and for panels c and d is 30-400 nm. Distributions are normalised to 30 ppbv naphthalene.

However, from 15 to 90 min, the SO_2-containing experiments consistently exhibit smaller mode diameters than the base case. This suggests that, although SO_2 promotes rapid nucleation and the formation of a large number of particles, the subsequent growth of each individual particle remains limited, consistent with the lower growth rates shown in Figure 7. One possible explanation is that sulfuric-acid-driven nucleation provides a large population of small particles onto which condensable compounds, including oxidation fragments and benzene-derived products, can partition. The available condensable material is therefore distributed among more particles, resulting in smaller final particle sizes.

In contrast, NO_x has the opposite effect on the dN/dlogD_p mode diameter. Although particle formation occurs later, NO_x enhances growth, leading to generally larger modes than in RM1. The maximum of the $dN/d\log D_p$ distribution is also elevated (typically by a factor of 4-6 relative to RM1), though not to the same extent as in the SO_2-containing mixtures. When both SO_2 and NO_x are present, particle number concentrations increase even more dramatically (350-600 times higher than the base case). In these cases, the mode remains larger than RM1 at early times (10-20 min) but becomes smaller at later times (30-150 min), reflecting the competing effects of rapid nucleation (from SO_2 addition) and enhanced growth (from NO_x addition). Finally, benzene generally reduces both $dN/d\log D_p$ concentrations (Figure 8) and growth rates (Figure 7), indicating a suppressive effect on particle formation due to benzene reacting with OH, resulting in slower oxidation of naphthalene.

https://doi.org/10.5194/egusphere-2026-6739
Preprint. Discussion started: 13 November 2026
© Author(s) 2026. CC BY 4.0 License.

SOA formation regimes

Particle formation and evolution, together with gas-phase chemical transformations, reveal four regimes across the eight reaction mixtures. These are summarised in Table 2.

Table 2. The four regimes identified among the investigated reaction mixtures and their averaged experimental parameters. Regime I consists of RM1 and RM3 (base case and benzene added). Regime II consists of RM2 and RM5 (NO_x added to Regime I). Regime III consists of RM4 and RM6 (SO_2 added to Regime I). Regime IV consists of RM7 and RM8 (co-addition of NO_x and SO_2 to Regime I). The values are in Mean (SE).

Regime	n_{PNC} ($\times 10^5$) / cm^{-3}	$t_{max,n}$ / min	r_{coag} / cm^3 s^{-1}	m_{SOA} / μg m^{-3}	$t_{max,m}$ / min	$m_{SOA}/m_{Nap,int}$ Ratio	r_{OH} ($\times 10^8$) / cm^{-3} s^{-1}
I: RM1, RM3	0.8 (0.2)	21.7 (2.9)	18.1 (5.0)	38.0 (5.8)	107.4 (3.9)	0.24 (0.04)	3.6 (0.8)
II: RM2, RM5	1.1 (0.3)	17.5 (2.3)	41.7 (16.0)	53.8 (4.2)	77.8 (9.3)	0.34 (0.03)	5.7 (1.3)
III: RM4, RM6	3.1 (0.6)	11.1 (1.4)	254.3 (142.8)	63.0 (23.8)	109.8 (5.8)	0.40 (0.15)	3.7 (0.8)
IV: RM7, RM8	5.6 (2.6)	7.5 (3.0)	888.3 (679.2)	106.2 (10.5)	75.4 (18.7)	0.67 (0.07)	5.6 (1.4)

The first regime (I) consists of RM1 and RM3, representing the base case and benzene addition. In this regime, particles form and subsequently grow. Benzene reduces the overall SOA mass expected from a mixture of 150 ppbv of organic compounds in comparison to RM1, which has 30 ppbv of organic compounds. However, it should be noted that the $m_{SOA}/m_{Nap,int}$ does not differ between the two reaction mixtures. Given that the OH concentration remains similar across the experiments, the possible reduction is attributed to kinetic competition, whereby benzene consumes OH while producing negligible SOA. This limits the OH available for naphthalene to form condensable products. This interpretation is consistent with the ToF-CIMS observations, where naphthalene oxidation products form later (Figure 6). Overall, compared with RM1, the changes observed in RM3 with respect to particle formation timescales are primarily driven by reduced OH availability, resulting in slower oxidation but not necessarily lower SOA mass produced.

The second regime (II) is characterised by the addition of only NO_x (RM2 and RM5) to the gas mixture. NO_x leads to faster SOA formation and an increase in particle mass, indicating faster and moderately enhanced SOA formation in the corresponding reaction mixture. The SOA produced per initial naphthalene in RM5 relative to RM3 is higher, which may indicate that benzene-derived oxidation products (or new products formed in the presence of NO_x) partition more efficiently when NO is present. Chen et al. 2016 report an increase in SOA mass as NO increased from 10-50 ppbv to 50-150 ppbv, followed by a decrease at higher NO. In an earlier study Chan et al. 2009 also observed less SOA formation at high NO_x (300-400 ppbv) than during experiments conducted in the absence of added NO_x. Overall, these studies suggest that moderate NO enhances SOA formation, with a maximum at intermediate NO/VOC, consistent with our results. At higher NO concentrations, SOA formation likely decreases (see Figure S49).

A corresponding increase in both the rate and magnitude of r_{coag} is also observed in Regime II, suggesting that higher NO_x coincides with higher n_{PNC} and enhanced r_{coag}. Compared to RM1, both RM2 and RM5 show consistently higher growth

https://doi.org/10.5194/egusphere-2026-6739
Preprint. Discussion started: 13 November 2026
© Author(s) 2026. CC BY 4.0 License.

rates, particularly for the smaller size intervals (Figure 7). Likewise, the $dN/d\log D_p$ mode evolution (Figure 8) indicates faster growth to larger mode diameters earlier in the experiment compared with the other regimes.

The addition of NO_x reduces the t_{max} times of m_{SOA}, r_{coag} and n_{PNC}. This effect is largest for m_{SOA}, moderate for r_{coag}, and weak for n_{PNC}. The same observation is made for selected oxidation products (Figure 6). Collectively, these results suggest that NO_x accelerates aerosol formation through faster oxidation processes. The OH production rate is nearly double that of Regime I; however, m_{SOA}/m_{Nap} does not increase by twice the amount, highlighting the non-linear nature of the relationship between OH production and recycling in the presence of NO_x and the formation of SOA. ToF-CIMS measurements further show that NO_x accelerates the formation of naphthalene oxidation products and introduces additional species into the oxidation product matrix, e.g., nitroaromatics. This means that more oxidised species form much faster, which studies (Tuet et al. (2017)) have found to be directly correlated with greater production of reactive oxygen and nitrogen species that could be harmful to human health.

The third regime (III) is defined by the addition of only SO_2 (RM4 and RM6). These experiments show increased particle mass concentrations, especially in the presence of benzene (RM6), as well as a higher m_{SOA}/m_{Nap} ratio in RM6, indicating that benzene-derived oxidation products may partition more efficiently under these reaction conditions. SO_2 enhances r_{coag} and n_{PNC} while reducing their t_{max}, consistent with rapid particle formation followed by efficient coagulation. In contrast, the time at which SOA reaches its maximum occurs later, and the OH production rate does not increase substantially in this regime. Similar studies (Liu et al., 2024; Yang et al., 2021) investigated the effects of SO_2 on aromatic photooxidation and observed higher production of SOA with respect to initial naphthalene concentrations, attributed to acid-catalysed heterogeneous reactions. This is consistent with our ToF-CIMS observations. Our results further indicate that SO_2 does not accelerate the formation of naphthalene oxidation products (in contrast to NO_x). Instead, species that were previously non-condensable appear to contribute more strongly after SO_2 addition. This effect is also evident when benzene is present: in RM3 benzene suppresses oxidation product formation by competing for OH, whereas in RM6 benzene-derived products appear to contribute additional SOA mass (Ben Brik et al., 2026). In RM3, the benzene oxidation products will remain in the gas-phase rather than partitioning into the particle phase as observed for RM6. Notably, SO_2 + OH alone did not yield detectable particles, whereas the addition of benzene resulted in particle formation, despite benzene + OH producing no detectable particles either with or without NO_x. This is consistent with Li et al. 2017, who showed that VOCs can promote SO_2 photooxidation and nucleation, followed by aerosol growth. Presumably, during VOC oxidation, the continual production of radicals (RO_2, HO_2) regenerates OH, which can react with SO_2 to produce sulfuric acid that nucleates with water to produce new particles that can subsequently grow.

The fourth regime (IV) involves the co-addition of SO_2 and NO_x (RM7 and RM8). Here, NO_x enhances OH production while SO_2 promotes the partitioning of previously non-condensable species to the particle phase. Together, these effects lead to highly efficient particle formation, with both higher concentrations and earlier peak times (Table 2). Liu et al. 2024 observed similarly synergistic effects of NO_x and SO_2, potentially through acid-catalysed heterogeneous reactions involving both nitric and sulfuric acid. Overall, these results highlight how co-emitted species can substantially influence aerosol formation in chemically complex systems relevant to occupational exposure (e.g., asphalt workplaces) and urban air quality. Details regarding

https://doi.org/10.5194/egusphere-2026-6739
Preprint. Discussion started: 13 November 2026
© Author(s) 2026. CC BY 4.0 License.

the chemical reaction pathways and oxidation products governing SOA formation in the regimes studied here will be reported in a follow-up study (Ben Brik et al., 202X).

4 Conclusions

Oxidation of individual SOA precursors is well documented, but real atmospheric environments rarely reflect such isolated conditions. It is therefore important to understand how co-emitted VOCs and inorganic gases affect the formation and subsequent growth of SOA. Here, we investigated a chemical system relevant to asphalt workplaces, where bitumen fumes may contain naphthalene together with benzene, NO_x, and SO_2 emitted during asphalt production or from nearby sources, using an experimental matrix of eight reaction mixtures. Adding benzene to the naphthalene + OH base case slowed SOA formation, consistent with competition for OH radicals and the production of comparatively less-condensable oxidation products. In contrast, adding benzene together with NO_x accelerated SOA formation. Adding SO_2 increased SOA formation, suggesting that benzene-derived products are converted into more condensable species or more easily partition into the particle phase under these conditions. More generally, SO_2 accelerated the onset of particle formation, although overall particle growth was reduced relative to the base case; importantly, SO_2 did not shift the timing of peak naphthalene oxidation products, indicating that earlier particle formation is driven primarily by enhanced partitioning rather than faster production of highly oxidized naphthalene products. NO_x substantially accelerated the formation of naphthalene oxidation products and advanced particle onset via more efficient OH recycling, but led to only a modest increase in SOA mass. The combined presence of NO_x and SO_2 produced the strongest overall effect, consistent with the additive effects of faster oxidation and enhanced partitioning to the particle phase.

Overall, these results demonstrate that the photo-oxidation of multi-component mixtures relevant to urban air and asphalt workplaces leads to SOA formation in ways that single-precursor experiments cannot predict. The experimental matrix revealed four distinct SOA formation regimes governed by interactions between benzene, NO_x and SO_2. Specifically, NO_x accelerated oxidation via enhanced OH recycling, while SO_2 promoted the condensation of oxidation products into the particle phase. Together, NO_x and SO_2 drove the strongest enhancement in organic aerosol mass and also activated SOA formation from benzene. Ultimately, these findings highlight that urban air quality and occupational exposures are dictated by complex chemical mixtures rather than isolated compounds. Future work will address the remaining questions regarding the chemical mechanisms, composition, and phase states of the aromatic oxidation products.

Code availability.

Available on request

Data availability.

https://doi.org/10.5194/egusphere-2026-6739
Preprint. Discussion started: 13 November 2026
© Author(s) 2026. CC BY 4.0 License.

Available on request

Code and data availability.

Available on request

Author contributions.

MP, ABB and NO'S performed the experiments with technical support from MCP, AAR and JW. MP and ABB processed and analysed the data. MP prepared the figures. MP and ABB wrote the original manuscript draft. All authors contributed to the conceptualization and methodology, and manuscript review. All authors discussed the results and approved the final manuscript.

Acknowledgements. The authors would like to warmly acknowledge Maarten Kieft and Lingshuo Meng for their contributions to this work, both with assistance in the laboratory and with discussions. We acknowledge that ChatGPT was used for proofreading and grammatical refinement of the text. It was also used to assist in optimising, debugging, and generalising MATLAB coding that was used. All generated code was manually reviewed, tested, and verified for accuracy by the authors.

This research was part of a Transnational access project supported by the European Commission under Horizon 2020 – Research and Innovation Framework Programme, H2020-INFRAIA-2020-1, ATMO-ACCESS Grant Agreement number 101008004. Support from Research Ireland's Frontiers for the Future Awards (21/FFP-A/8973) and by FFIKA2, a grant from the Danish Government 2023-2026 are also gratefully acknowledged.

https://doi.org/10.5194/egusphere-2026-6739
Preprint. Discussion started: 13 November 2026
© Author(s) 2026. CC BY 4.0 License.

References

Abue, P., Bhattacharyya, N., Tang, M., Jahn, L. G., Blomdahl, D., Allen, D. T., Corsi, R. L., Novoselac, A., Mistzal, P. K., and Hildebrandt Ruiz, L.: Emissions from Hydrogen Peroxide Disinfection and Their Interaction with Mask Surfaces, ACS Engineering Au, 4, 204–212, 2024.

Borrás, E. and Tortajada-Genaro, L. A.: Secondary organic aerosol formation from the photo-oxidation of benzene, Atmospheric Environment, 47, 154–163, 2012.

Burstyn, I., Randem, B., Lien, J. E., Langård, S., and Kromhout, H.: Bitumen, polycyclic aromatic hydrocarbons and vehicle exhaust: exposure levels and controls among Norwegian asphalt workers, Annals of occupational hygiene, 46, 79–87, 2002.

Chan, A. W. H., Kautzman, K. E., Chhabra, P. S., Surratt, J. D., Chan, M. N., Crounse, J. D., Kürten, A., Wennberg, P. O., Flagan, R. C., and Seinfeld, J. H.: Secondary organic aerosol formation from photooxidation of naphthalene and alkylnaphthalenes: implications for oxidation of intermediate volatility organic compounds (IVOCs), Atmospheric Chemistry and Physics, 9, 3049–3060, https://doi.org/10.5194/acp-9-3049-2009, 2009.

Chen, C.-L., Kacarab, M., Tang, P., and Cocker III, D. R.: SOA formation from naphthalene, 1-methylnaphthalene, and 2-methylnaphthalene photooxidation, Atmospheric Environment, 131, 424–433, 2016.

Chen, C.-L., Li, L., Tang, P., and Cocker III, D. R.: SOA formation from photooxidation of naphthalene and methylnaphthalenes with m-xylene and surrogate mixtures, Atmospheric Environment, 180, 256–264, 2018.

Cheng, Q., Zhang, Y., Chen, D., Zhang, T., Yang, K., Wang, J., Jiang, H., Liu, P., Wang, Z., He, Y., et al.: Distinguishing Primary and Secondary Tracers to Quantify Naphthalene and Methylnaphthalene Contributions to Secondary Organic Aerosol in the Pearl River Delta, Atmosphere, 17, 354, 2026.

del Carmen Rubio, M., Moreno, F., Martínez-Echevarría, M. J., Martínez, G., and Vázquez, J. M.: Comparative analysis of emissions from the manufacture and use of hot and half-warm mix asphalt, Journal of cleaner production, 41, 1–6, 2013.

Elihn, K., Ulvestad, B., Hetland, S., Wallén, A., and Randem, B. G.: Exposure to ultrafine particles in asphalt work, Journal of occupational and environmental hygiene, 5, 771–779, 2008.

Freund, A., Zuckerman, N., Baum, L., and Milek, D.: Submicron particle monitoring of paving and related road construction operations, Journal of occupational and environmental hygiene, 9, 298–307, 2012.

Hedmer, M., Lovén, K., Rex, J., Nilsson, C. A., Polat, M., Nøjgaard, J. K., Pagels, J., Strandberg, B., and Hagvall, L.: Characterization of occupational exposure to air pollutants during asphalt milling and paving, Annals of Work Exposures and Health, 70, wxaf078, 2026.

Huang, G., Liu, Y., Shao, M., Li, Y., Chen, Q., Zheng, Y., Wu, Z., Liu, Y., Wu, Y., Hu, M., et al.: Potentially important contribution of gas-phase oxidation of naphthalene and methylnaphthalene to secondary organic aerosol during haze events in Beijing, Environmental science & technology, 53, 1235–1244, 2019.

Kautzman, K., Surratt, J., Chan, M., Chan, A., Hersey, S., Chhabra, P., Dalleska, N., Wennberg, P., Flagan, R., and Seinfeld, J.: Chemical composition of gas-and aerosol-phase products from the photooxidation of naphthalene, The Journal of Physical Chemistry A, 114, 913–934, 2010.

Khare, P. and Gentner, D. R.: Considering the future of anthropogenic gas-phase organic compound emissions and the increasing influence of non-combustion sources on urban air quality, Atmospheric Chemistry and Physics, 18, 5391–5413, https://doi.org/10.5194/acp-18-5391-2018, 2018.

https://doi.org/10.5194/egusphere-2026-6739
Preprint. Discussion started: 13 November 2026
© Author(s) 2026. CC BY 4.0 License.

Khare, P., Machesky, J., Soto, R., He, M., Presto, A. A., and Gentner, D. R.: Asphalt-related emissions are a major missing nontraditional source of secondary organic aerosol precursors, Science advances, 6, eabb9785, 2020.

Kleindienst, T. E., Jaoui, M., Lewandowski, M., Offenberg, J. H., and Docherty, K. S.: The formation of SOA and chemical tracer compounds from the photooxidation of naphthalene and its methyl analogs in the presence and absence of nitrogen oxides, Atmospheric Chemistry and Physics, 12, 8711–8726, 2012.

Kriech, D. M., Crawford, A. C., Smith, L. A., Osborn, L. V., and Kriech, A. J.: Characterizing asphalt emissions under in-service conditions, Atmospheric Environment: X, 16, 100 196, 2022.

Lannuque, V. and Sartelet, K.: Development of a detailed gaseous oxidation scheme of naphthalene for secondary organic aerosol (SOA) formation and speciation, Atmospheric Chemistry and Physics, 24, 8589–8606, 2024.

Li, J., Li, K., Zhang, H., Zhang, X., Ji, Y., Chu, W., Kong, Y., Chu, Y., Ren, Y., Zhang, Y., et al.: Effects of OH radical and SO_2 concentrations on photochemical reactions of mixed anthropogenic organic gases, Atmospheric Chemistry and Physics, 22, 10 489–10 504, 2022.

Li, J., Qin, Y., Zhang, X., Shan, B., and Liu, C.: Emission characteristics, environmental impacts, and health risks of volatile organic compounds from asphalt materials: A state-of-the-art review, Energy & Fuels, 38, 4787–4802, 2024.

Li, K., Chen, L., White, S. J., Han, K., Lv, B., Bao, K., Wu, X., Gao, X., Azzi, M., and Cen, K.: Effect of nitrogen oxides (NO and NO_2) and toluene on SO_2 photooxidation, nucleation and growth: A smog chamber study, Atmospheric research, 192, 38–47, 2017.

Liu, S., Wang, Y., Zhang, S., Chen, Y., Wu, C., Zhang, G., and Wang, G.: The synergistic effect of NO_x and SO_2 on the formation and light absorption of secondary organic aerosols from o-xylene photooxidation, Atmospheric Research, 304, 107 387, 2024.

Mousavi, M., Emrani, J., Teleha, J. C., Jiang, G., Johnson, B. D., Shamshiripour, A., and Fini, E. H.: Health risks of asphalt emission: State-of-the-art advances and research gaps, Journal of Hazardous Materials, 480, 136 048, 2024.

Riva, M., Robinson, E. S., Perraudin, E., Donahue, N. M., and Villenave, E.: Photochemical aging of secondary organic aerosols generated from the photooxidation of polycyclic aromatic hydrocarbons in the gas-phase, Environmental science & technology, 49, 5407–5416, 2015.

Sari Doré, F., Carstens, C., Top, J., Zhang, Y., Dubois, C., Perrier, S., El Haddad, I., Bell, D. M., and Riva, M.: Photodegradation of naphthalene-derived particle oxidation products, Environmental Science: Atmospheres, 5, 300–315, 2025.

Seinfeld, J. H. and Pandis, S. N.: Atmospheric chemistry and physics: from air pollution to climate change, John Wiley & Sons, 2016.

Shakya, K. M. and Griffin, R. J.: Secondary organic aerosol from photooxidation of polycyclic aromatic hydrocarbons, Environmental science & technology, 44, 8134–8139, 2010.

Spicer, C. W., Joseph, D. W., and Ollison, W. M.: A re-examination of ambient air ozone monitor interferences, Journal of the Air & Waste Management Association, 60, 1353–1364, 2010.

Tuet, W. Y., Chen, Y., Xu, L., Fok, S., Gao, D., Weber, R. J., and Ng, N. L.: Chemical oxidative potential of secondary organic aerosol (SOA) generated from the photooxidation of biogenic and anthropogenic volatile organic compounds, Atmospheric Chemistry and Physics, 17, 839–853, 2017.

Väänänen, V., Hämeilä, M., Kontsas, H., Peltonen, K., and Heikkilä, P.: Air concentrations and urinary metabolites of polycyclic aromatic hydrocarbons among paving and remixing workers, Journal of Environmental Monitoring, 5, 739–746, 2003.

Yang, Z., Tsona, N. T., Li, J., Wang, S., Xu, L., You, B., and Du, L.: Effects of NO_x and SO_2 on the secondary organic aerosol formation from the photooxidation of 1, 3, 5-trimethylbenzene: A new source of organosulfates, Environmental pollution, 264, 114 742, 2020.

Yang, Z., Xu, L., Tsona, N. T., Li, J., Luo, X., and Du, L.: SO_2 and NH_3 emissions enhance organosulfur compounds and fine particle formation from the photooxidation of a typical aromatic hydrocarbon, Atmospheric Chemistry and Physics, 21, 7963–7981, 2021.

https://doi.org/10.5194/egusphere-2026-6739
Preprint. Discussion started: 13 November 2026
© Author(s) 2026. CC BY 4.0 License.



Zhang, W., Wang, W., Li, J., Peng, C., Li, K., Zhou, L., Shi, B., Chen, Y., Liu, M., and Ge, M.: Effects of SO_2 on optical properties of secondary organic aerosol generated from photooxidation of toluene under different relative humidity conditions, Atmospheric Chemistry and Physics, 20, 4477–4492, 2020.